organization, and functional expression of Na^+/H^+ exchanger isoform 5 (NHE5) from human brain, *J. Biol. Chem. 274*, 4377−4382.
10. Goyal, S., Vanden Heuvel, G., and Aronson, P. S. (2003) Renal expression of novel Na^+/H^+ exchanger isoform NHE8, *Am. J. Physiol. 284*, F467−473.
11. Lin, X., and Barber, D. L. (1996) A calcineurin homologous protein inhibits GTPase-stimulated Na−H exchange, *Proc. Natl. Acad. Sci. U.S.A. 93*, 12631−12636.
12. Pang, T., Su, X., Wakabayashi, S., and Shigekawa, M. (2001) Calcineurin homologous protein as an essential cofactor for Na^+/H^+ exchangers, *J. Biol. Chem. 276*, 17367−17372.
13. Pang, T., Wakabayashi, S., and Shigekawa, M. (2002) Expression of calcineuin B homologous protein 2 protects serum deprivaion-induced cell death by serum-independent activation of Na^+/H^+ exchanger, *J. Biol. Chem. 277*, 43771−43777.
14. Bertrand, B., Wakabayashi, S., Ikeda, T., Pouysségur, J., and Shigekawa, M. (1994) The Na^+/H^+ exchanger isoform 1 (NHE1) is a novel member of the calmodulin-binding proteins: Identification and characterization of calmodulin-binding sites, *J. Biol. Chem. 269*, 13703−13709.
15. Wakabayashi, S., Bertrand, B., Ikeda, T., Pouysségur, J., and Shigekawa, M. (1994) Mutation of calmodulin-binding site renders the Na^+/H^+ exchanger (NHE1) highly H^+-sensitive and Ca^{2+} regulation-defective, *J. Biol. Chem. 269*, 13710−13715.
16. Voyno-Yasenetskaya, T., Conklin, B. R., Gilbert, R. L., Hooley, R., Bourne, H. R., and Barber, D. L. (1994) G alpha 13 stimulates Na−H exchange, *J. Biol. Chem. 269*, 4721−4724.
17. Bianchini, L., L'Allemain, G., and Pouysségur, J. (1997) The p42/p44 Mitogen-activated protein kinase cascade is determinant in mediating activation of the Na^+/H^+ exchanger (NHE1 isoform) in response to growth factors, *J. Biol. Chem. 272*, 271−279.
18. Takahashi, E., Abe, J.-I., Gallis, B., Aebersold, R., Spring, D. J., Krebs, E. G., and Berk, B. C. (1999) $p90^{RSK}$ is a serum-stimulated Na^+/H^+ exchanger isoform-1 kinase. Regulatory phosphorylation of serine 703 of Na^+/H^+ exchanger isoform-1, *J. Biol. Chem. 274*, 20206−20214.
19. Lehoux, S., Abe, J. I., Florian, J. A., and Berk, B. C. (2001) 14-3-3 binding to Na^+/H^+ exchanger isoform-1 is associated with serum-dependent activation of Na^+/H^+ exchange, *J. Biol. Chem. 276*, 15794−15800.
20. Yan, W., Nehrke, K., Choi, J., and Barber, D. L. (2001) The Nck-interacting kinase (NIK) phosphorylates the Na^+-H^+ exchanger NHE1 and regulates NHE1 activation by platelet-derived growth factor, *J. Biol. Chem. 276*, 31349−31356.
21. Aharonovitz, O., Zaun, H. C., Balla, T., York, J. D., Orlowski, J., and Grinstein, S. (2000) Intracellular pH regulation by Na^+/H^+ exchange requires phosphatidylinositol 4,5-bisphosphate, *J. Cell Biol. 150*, 213−224.
22. Li, X., Alvarez, B., Casey, J. R., Reithmeier, R. A. F., and Fliegel, L. (2002) Carbionic anhydrase II binds to and enhances activity of the Na^+/H^+ exchanger, *J. Biol. Chem. 277*, 36085−36091.
23. Barroso, M. R., Bernd, K. K., DeWitt, N. D., Chang, A., Mills, K., and Sztul, E. S. (1996) A novel Ca^{2+}-binding protein, p22, is required for constitutive membrane traffic, *J. Biol. Chem. 271*, 10183−10187.
24. Lin, X., Sikkink, R. A., Rusnak, F., and Barber, D. L. (1999) Inhibition of calcineurin phosphatase activity by a calcineurin B homologous protein, *J. Biol. Chem. 274*, 36125−36131.
25. Timm, S., Titus, B., Bernd, K., and Barroso, M. (1999) The EF-hand Ca^{2+}-binding protein p22 associates with microtubules in an N-myristoylation-dependent manner, *Mol. Biol. Cell 10*, 3473−3488.
26. Matsumoto, M., Miyake, Y., Nagita, M., Inoue, H., Shitakubo, D., Takemoto, K., Ohtsuka, C., Murakami, H., Nakamura, N., and Kanazawa, H. (2001) A serine/threonine kinase which causes apoptosis-like cell death interacts with a calcineurin B-like protein capable of binding Na^+/H^+ exchanger, *J. Biochem. (Tokyo) 130*, 217−225.
27. Nakamura, N., Miyake, Y., Matsushita, M., Tanaka, S., Inoue, H., and Kanazawa, H. (2002) KIF1Bβ2, capable of interacting with CHP, is localized to synaptic vesicles, *J. Biochem. (Tokyo) 132*, 483−492.
28. Inoue, H., Nakamura, Y., Nagita, M., Takai, T., Masuda, M., Nakamura, N., and Kanazawa, H. (2003) Calcineurin homologous protein isoform 2 (CHP2), Na^+/H^+ exchangers-binding protein, is expressed in intestinal epithelium, *Biol. Pharm. Bull. 26* (2), 148−155.
29. Pouysségur, J., Sardet, C., Franchi, A., L'Allemain, G., and Paris, S. (1984) A specific mutation abolishing Na^+/H^+ antiport activity in hamster fibroblasts precludes growth at nertral and acidic pH, *Proc. Natl. Acad. Sci. U.S.A. 81*, 4833−4837.
30. Wakabayashi, S., Fafournoux, P., Sardet, C., and Pouysségur, J. (1992) The Na^+/H^+ antiporter cytoplasmic domain mediates growth factor signals and controls "H^+-sensing", *Proc. Natl. Acad. Sci. U.S.A. 89*, 2424−2428.
31. Wakabayashi, S., Ogurusu, T., and Shigekawa, M. (1986) Factors influencing calcium release from the ADP-sensitive phosphoenzyme intermediate of the sarcoplasmic reticulum ATPase, *J. Biol. Chem. 261*, 9762−9769.
32. Ikeda, T., Schmitt, B., Pouysségur, J., Wakabayashi, S., and Shigekawa, M. (1997) Identification of cytoplasmic subdomains that control pH-sensing of theNa^+/H^+ exchanger (NHE1): pH-maintenance, ATP-sensitive, and flexible loop domains, *J. Biochem. (Tokyo) 121*, 295−303.
33. Strynadka, N. C. J., and James, M. N. G. (1989) Crystal structures of the helix-loop-helix calcium-binding proteins, *Annu. Rev. Biochem. 58*, 951−998.
34. Yap, K. L., Ames, J. B., Swindells, M. B., and Ikura, M. (1999) Diversity of conformational states and changes within the EF-hand protein superfamily, *Proteins 37*, 499−507.
35. Szebenyi, D. M. E., Obendorf, S. K., and Moffat, K. (1981) Structure of vitamin D-dependent calcium-binding protein from bovine intestine, *Nature 294*, 327−332.
36. Stemmer, P. M., and Klee, C. B. (1994) Dual Calcium Ion Regulation of Calcineurin by Calmodulin and Calcineurin B, *Biochemistry 33*, 6859−6866.
37. Pauls, T. L., Durussel, I., Cox, J. A., Clark, I. D., Szabo, A. G., Gagne, S. M., Sykes, B. D., and Berchtold, M. W. (1993) Metal binding properties of recombinant rat parvalbumin wild-type and F102W mutant, *J. Biol. Chem. 268*, 20897−20903.
38. Gross, M. D., Gosnell, M., Tsarbopoulos, A., and Hunziker, W. (1993) A functional and degenerate pair of EF hands contains the very high affinity calcium-binding site of calbindin-D_{28K}, *J. Biol. Chem. 268*, 20917−20992.
39. Burgoyne, R. D., and Weiss, J. L. (2001) The neuronal calcium sensor family of Ca^{2+}-binding proteins, *Biochem. J. 353*, 1−12.
40. Olwin, B. B., Edelman, A. M., Krebs, E. G., and Storm, D. R. (1984) Quantitation of energy coupling between Ca^{2+}, calmodulin, skeletal muscle myosin light chain kinase, and kinase substrates, *J. Biol. Chem. 259*, 10949−10955.
41. Johnson, J. D., Snyder, C., Walsh, M., and Flynn, M. (1996) Effects of myosin light chain kinase and peptides on Ca^{2+} exchange with the N- and C-terminal Ca^{2+} binding sites of calmodulin, *J. Biol. Chem. 271*, 761−767.
42. Feng, B., and Stemmer, P. M. (1999) Interactions of calcineurin A, calcineurin B, and Ca^{2+}, *J. Biol. Chem. 38*, 12481−12489.
43. Kissinger, C. R., Parge, H. E., Knighton, D. R., Lewis, C. T., Pelletier, L. A., Tempczyk, A., Kalish, V. J., Tucker, K. D., Showalter, R. E., Moomaw, E. W., Gastinel, L. N., Habuka, N., Chen, X., Maldonado, F., Barker, J. E., Bacquet, R., and Villafranca, J. E. (1995) Crystal structures of human calcineurin and the human FKBP12−FK506-calcineurin complex, *Nature 378*, 641−644.
44. Wakabayashi, S., Hisamitsu, T., Pang, T., and Shigekawa, M. (2003) Mutations of Arg^{440} and Gly^{455}/Gly^{456} oppositely change pH sensing of Na^+/H^+ exchanger 1, *J. Biol. Chem. 278*, 11828−11835.
45. Garnovaskaya, M. N., Mukhin, Y. V., Vlasova, T. M., and Raymond, J. R. (2003) Hypertonicity activates Na^+/H^+ exchange through Janus kinase 2 and calmodulin, *J. Biol. Chem. 278*, 16908−16915.
46. Mukhin, Y. V., Vlasova, T., Jaffa, A. A., Collinsworth, G., Bell, J. L., Tholanikunnel, B. G., Petus, T., Fitzgibbon, W., Ploth, D. W., Raymond, J. R., and Garnovskaya, M. N. (2001) Bradykinin B_2 receptors activate Na^+/H^+ exchange in mIMCD-3 cells via Janus kinase 2 and Ca^{2+}/calmodulin, *J. Biol. Chem. 276*, 17339−17346.
47. Robertson, M. A., Woodside, M., Foskett, J. K., Orlowski, J., and Grinstein, S. (1997) Muscarinic agonists induce phosphorylation-independent activation of the NHE−1 isoform of the Na^+/H^+ antiporter in salivary acinar cells, *J. Biol. Chem. 272*, 287−294.
48. Moor, AN, Murtazina, R, and Fliegel, L. (2000) Calcium and osmotic regulation of the Na^+/H^+ exchanger in neonatal ventricular myocytes, *J. Mol. Cell. Cardiol. 32*, 925−936.

BI0360004

In Situ Measurements of Crossbridge Dynamics and Lattice Spacing in Rat Hearts by X-Ray Diffraction

Sensitivity to Regional Ischemia

James T. Pearson, PhD; Mikiyasu Shirai, MD, PhD; Haruo Ito, PhD; Noriyuki Tokunaga, MD; Hirotsugu Tsuchimochi, PhD; Naoki Nishiura; Daryl O. Schwenke, PhD; Hatsue Ishibashi-Ueda, MD; Ryuichi Akiyama, PhD; Hidezo Mori, MD, PhD; Kenji Kangawa, PhD; Hiroyuki Suga, MD, PhD; Naoto Yagi, PhD

Background—Synchrotron radiation has been used to analyze crossbridge dynamics in isolated papillary muscle and excised perfused hearts with the use of x-ray diffraction techniques. We showed that these techniques can detect regional changes in rat left ventricle contractility and myosin lattice spacing in in situ ejecting hearts in real time. Furthermore, we examined the sensitivity of these indexes to regional ischemia.

Methods and Results—The left ventricular free wall of spontaneously beating rat hearts (heart rate, 290 to 404 bpm) was directly exposed to brief high-flux, low-emittance x-ray beams provided at SPring-8. Myosin mass transfer to actin filaments was determined as the decrease in reflection intensity ratio (intensity of 1,0 plane over the 1,1 plane) between end-diastole and end-systole. The distance between 1,0 reflections was converted to a lattice spacing between myosin filaments. We found that mass transfer (mean, 1.71±0.09 SEM, n=13 hearts) preceded significant increases in lattice spacing (2 to 5 nm) during systole in nonischemic pericardium. Left coronary occlusion eliminated increases in lattice spacing and severely reduced mass transfer ($P<0.01$) in the ischemic region.

Conclusions—Our results suggest that x-ray diffraction techniques permit real-time in situ analysis of regional crossbridge dynamics at molecular and fiber levels that might also facilitate investigations of ventricular output regulation by the Frank-Starling mechanism. **(*Circulation*. 2004;109:2976-2979.)**

Key Words: ischemia ■ myocardial contraction ■ myosin ■ radiography

Despite the history of studies on crossbridge dynamics, lower photon counts and poorer quality of diffraction patterns obtained from cardiac muscle than skeletal and insect flight muscles[1–3] have limited progress with cardiac muscle until recently.[4,5] Some of us used third-generation synchrotron radiation (SPring-8, Japan Synchrotron Radiation Research Institute) to determine x-ray diffraction patterns in excised, perfused rat hearts while moving systematically across the left ventricular (LV) equator from the epicardium through to the ventricular cavity.[6]

X-ray diffraction patterns of cardiac muscle produce 2 equatorial-position reflections from the lattice-like arrangement of its protein elements.[2] Mass transfer of myosin heads to actin during contraction is inferred from a decrease in the integrated 1,0 reflection intensity ($I_{1,0}$, lattice plane containing only thick myosin filaments) and an increase in 1,1 reflection intensity ($I_{1,1}$, plane with thick myosin and thin actin filaments).[7] The myocardial intensity ratio (defined as $I_{1,0}/I_{1,1}$) is minimal in the rigor state and maximal in a quiescent state.[1,2,6,8]

Furthermore, the distance between 1,0 reflection peaks ($d_{1,0}$ spacing) represents the myosin lattice spacing, which is inversely related to sarcomere length in isolated fibers[5] as static myocytes maintain a constant cell volume. Whether decreases in myofilament spacing contribute to increasing Ca^{2+} sensitivity and increased probability of crossbridge formation at longer sarcomere lengths has been actively debated.[9] However, it is still not known if lattice spacing is regulated to maintain constant lattice volume (ie, if lattice cross-sectional area decreases with increasing sarcomere length, then interfilament spacing must decrease) during dynamic contractions in vivo.

Recently, it was shown that the intensity ratio derived from x-ray diffraction patterns of isolated whole hearts decreased during isovolumic contractions with a similar time course throughout the LV,[6] implying that crossbridge cycling in fibers of different myocardial layers is similar despite differences in fiber orientation and rate of short-

Received March 1, 2004; de novo received March 31, 2004; revision received May 6, 2004; accepted May 6, 2004.

From the National Cardiovascular Center Research Institute, Osaka, Japan (J.T.P., M.S., N.T., H.T., N.N., D.O.S., H.I.-U., H.M., K.K., H.S.); S-I Medico-Tech Co Ltd, Kashiwara, Osaka, Japan (H.I.); Muroran Institute of Technology, Muroran, Japan (R.A.); and SPring-8/JASRI, Sayo, Hyogo, Japan (N.Y.)

Correspondence to Dr James T. Pearson, Cardiac Physiology, National Cardiovascular Center Research Institute, 5-7-1 Fujishirodai, Suita, Osaka 565-8565 Japan. E-mail jpearson@ri.ncvc.go.jp

Circulation is available at http://www.circulationaha.org

DOI: 10.1161/01.CIR.0000133322.19340.EF

ening. However, it was not possible to follow dynamic lattice spacing changes. In the present study, we used a fine-focused x-ray beam to record diffraction patterns of a localized region of the LV of ejecting rat hearts in situ and then determined crossbridge cycling and myosin lattice spacing.

Methods

Animals and Surgical Preparation

Anesthetized (50 mg/kg sodium pentobarbital IP) male Sprague-Dawley rats (Japan SLC, Hamamatsu, Japan), 9 to 10 weeks of age (350 to 400 g), were artificially ventilated and thoractomized. Procedures were performed according to SPring-8 guidelines for the care and welfare of experimental animals. The heart was continuously irrigated while the apex was raised by a manipulator paddle and restrained by 2 superficial sutures in the LV to minimize vertical movements. Pressure-volume loops were recorded from an apically inserted 1.4F micromanometer (SPR-671 Millar Instruments) and a 1.5F conductance catheter (S-I Medico-tech Co Ltd. Osaka)[10] to determine the temporal sequence of cardiac events and heart rate (determined from end-diastole [ED] interval).

X-Ray Diffraction With Collimated Synchrotron Radiation

Measurements were conducted at the 40XU beamline of SPring-8.[6] A collimated quasimonochromatic beam (wavelength, 0.08 nm) with a beam flux of $\approx 10^{12}$ photons per second (15 keV; ring current, 60 to 100 mA) and dimensions 0.2 × 0.2 mm was focused at an oblique tangent to the myocardium ($\approx$3 m from the detector). The ventilator was stopped at end-expiration to reduce heart movements during measurements ($\approx$2.1 seconds). Images were digitally recorded at a 15-ms sampling interval with the use of an image intensifier and a fast CCD camera,[6] simultaneous with pressure-volume analog signals (1000-Hz sampling frequency). The beam passed through the apical myocardium between the ends of the descending branch of the left coronary artery (LAD) and the posterior interventricular vein. Final burning of the recorded region (higher energy levels) confirmed that the beam only exposed fibers in the epicardium and part of the intermediate layer (histological inspection).

Acute Ischemia Treatment

Heart baseline recordings were established, permanent ligation of the proximal LAD was performed, and recordings were repeated 5 to 10 minutes later.

Intensity Ratio Calculations and Analyses

Integrated intensity of $I_{1,0}$ and $I_{1,1}$ was determined from the areas under the reflection peaks after background subtraction.[6] Intensity ratio ($I_{1,0}/I_{1,1}$) was used rather than absolute reflection intensities of $I_{1,0}$ and $I_{1,1}$, which are influenced by changes in the quantity of fibers sampled during contractions.[3] Myosin mass transfer index was defined as the difference in intensity ratio between ED and end systole (ES).

Results

Mass Transfer and Lattice Spacing in Nonischemic Hearts

Intensity ratio significantly decreased during systole (increase in LV pressure [LVP] and decrease in LV volume [LVV]) and conversely, increased during diastole under the baseline rhythm (Figure 1a). Averaging intensity ratio over multiple beats reduced variability during diastole in the otherwise sinusoidal patterns (black lines, Figure 1b). With regard to time, $d_{1,0}$ spacing increased continuously

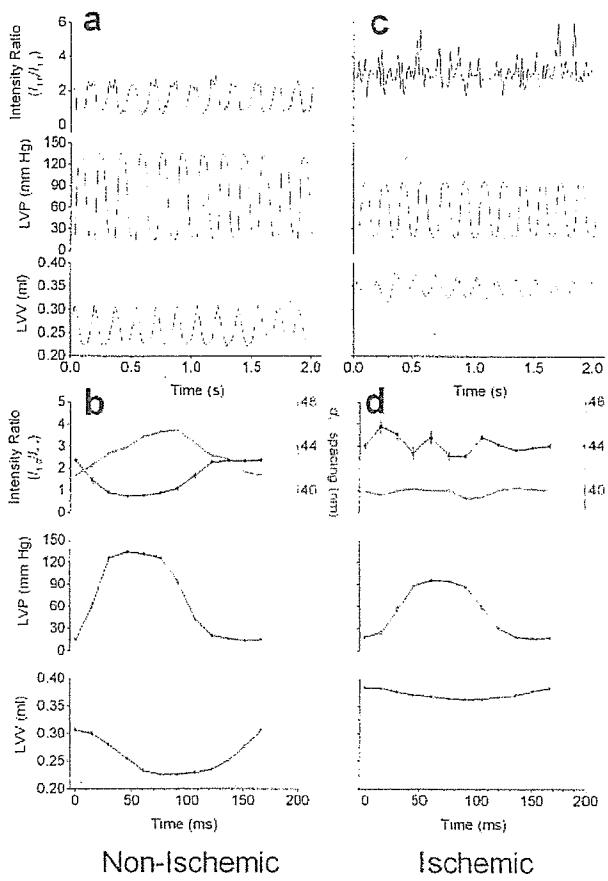

Figure 1. Relations between calculated intensity ratio, $d_{1,0}$ spacing, LVP, and LVV obtained from an LV with the use of x-ray diffraction. a and c, Consecutive records (15-ms intervals) of intensity ratio, LVP, and LVV during the baseline (a) and after LAD occlusion (c) in the same heart. b and d, Average changes in intensity ratio (black lines), $d_{1,0}$ spacing (red lines), LVP, and LVV over the cardiac cycle between the ED events (derived from a and c, respectively; bars indicate SEM).

during systole and then decreased during diastole, suggesting that considerable changes occur in the myofilament spacing (red line, Figure 1b).

Intensity ratio averaged 2.80±0.11 (SEM, n=13 hearts) at ED, and the average myosin mass transfer index was 1.71±0.09. In all hearts, the decrease in intensity ratio during crossbridge formation was completed before the full extent of the $d_{1,0}$ spacing change (2 to 5 nm between hearts, Figure 2a). Furthermore, at any given LVV, the $d_{1,0}$ spacing during systole was 1 to 2 nm larger than diastole (Figure 2b).

Mass Transfer and Lattice Spacing During Regional Ischemia

LAD occlusion reduced the intensity ratio change and prevented normal lattice spacing increase, consistent with reduced contractility of the ischemic region (Figure 1, c and d). Occlusion significantly increased intensity ratios at both ED ($P<0.05$) and ES ($P<0.001$) in the same LV region (n=6,

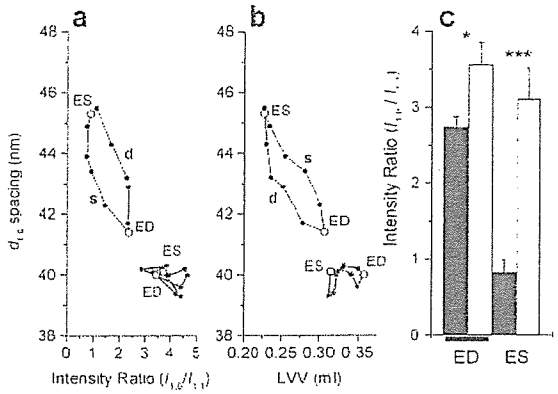

Figure 2. a and b, Average loops formed between $d_{1,0}$ spacing, LVV, and intensity ratio during consecutive cycles (shown in Figure 1) under baseline conditions (black symbols) and regional ischemia (red symbols). Systolic (s) and diastolic (d) trajectories are indicated for baseline. c, Mean intensity ratio at ED and ES during baseline (black columns) and regional ischemia (open columns; group mean±SEM). Ischemia versus baseline, paired *t* test *$P<0.05$, ***$P<0.001$.

Figure 2c). Although mean heart rate was not depressed (341±16 bpm, 4% increase) and there was only a small decrease in mean LV ES pressure (−26.9±5.8 mm Hg SEM), regional ischemia severely depressed the mass transfer index (55% of baseline).

Discussion

Our data clearly demonstrate that current synchrotron technology can produce sufficient energy to obtain well-defined reflections from single exposures to enable calculation of intensity ratio and $d_{1,0}$ spacing in in situ rat hearts (Figure 1). The mean ED intensity ratio of this study is similar to 2.96 obtained from LV in arrested rat hearts under normoxic perfusion.[8] Furthermore, in rat papillary muscles, the resting ratio was 3.07.[1,2] The results presented here were restricted to epicardial recordings (within 0.8-mm depth), consisting of helically orientated fibers, to minimize the contributions from fibers with orientations that vary at greater depth.[11] Nevertheless, it was recently established that neither diastolic intensity ratio nor mass transfer varies with depth of x-ray beam penetration in beating, perfused hearts (paced at 2 Hz).[6]

In Situ Changes in Myofilament Spacing

We showed that significant lattice expansion occurs during contraction and that the relation between $d_{1,0}$ spacing and intensity ratio is not linear but a loop in nonischemic hearts (black line, Figure 2a). The $d_{1,0}$ spacing changes during contraction (2 to 5 nm) were larger than the 1-nm difference in $d_{1,0}$ spacing reported between the epicardium and endocardium (at diastole).[6] Therefore, the larger $d_{1,0}$ spacing change found in ejecting hearts cannot be explained by shifts in the fiber layers exposed to the beam. The loop formed by these indexes might contain valuable information about how crossbridge axial and radial forces alter the dynamics of lattice spacing changes. Crossbridge projections from the myosin backbone produce radial force perpendicular to that of axial force in the filament direction.[12] Release of isometric tension in intact skeletal myofibers during sarcomere shortening causes a brief and rapid lattice spacing increase, in excess of that predicted by fiber shortening in itself.[12,13] We therefore conclude that lattice volume is not constant in the dynamic state because myosin lattice spacing is significantly larger (1 to 2 nm) during contraction than ventricular filling at the same LVV ($d_{1,0}$ spacing during systole greater than diastole, Figure 2b). Crossbridge formation probably causes a brief lattice expansion in ejecting hearts mediated by radial forces.

Sensitivity of In Situ Indexes to Regional Ischemia

The relevance of our new findings is that although the intensity ratio of beating hearts in diastole was similar to that of relaxed papillary muscles, there is a very different response of the myocardium in beating hearts to ischemia in terms of crossbridge dynamics and lattice space changes. Higher intensity ratios and more variable intensity ratio changes during systole (Figure 1, c and d) occurred as the result of lower absolute $I_{1,1}$ in systole and a lack of consistent increase in $I_{1,1}$ when $I_{1,0}$ decreased (data not shown). Thus, permanent regional ischemia severely attenuated mass transfer in the epicardium (Figure 2c). Furthermore, ischemia induced increases in ED intensity ratio in vivo, whereas other studies report maximal decreases in the intensity ratio under anoxic perfusion (isolated arrested hearts)[8] or rigor.[1,2] An increase in intensity ratio might be related to metabolite accumulation or pronounced passive stretching, because fiber shortening in infarcted regions progressively decreases until fibers eventually become passively stretched (bulging) by fiber shortening in the nonischemic region.[14] In support of the bulging possibility, we found that $d_{1,0}$ spacing no longer increases between ED and ES after occlusion.

The cellular basis of the Frank-Starling law of the heart involves increases in contractility caused by length-dependent increases in Ca^{2+} sensitivity associated with increased ventricular filling.[9] However, it is still debated whether increased crossbridge activation results from increased probability of crossbridge formation with decreasing lattice spacing associated with fiber stretching (see review in Reference 9). In a future publication, we will examine how LV volume loading influences mass transfer in relation to myofilament spacing and length-dependent activation of contraction in situ.

Acknowledgments

This work was supported by the Promotion of Fundamental Studies in Health Sciences of the Organization for Pharmaceutical Safety and Research (OPSR) and Ministerial grants Nano-001 and a Grant-in-Aid for Scientific Research. The experiments were made with approval of the SPring-8 Program Review Committee. We thank Dr Keiji Umetani for access to the Medical Imaging Center.

References

1. Matsubara I, Kamiyama A, Suga H. X-ray diffraction study of contracting heart muscle. *J Mol Biol*. 1977;111:121–128.
2. Matsubara I, Suga H, Yagi N. An X-ray diffraction study of the cross-circulated canine heart. *J Physiol (London)*. 1977;270:311–320.

3. Yagi N, Saeki Y, Ishikawa T, et al. Cross-bridge and calcium behavior in ferret papillary muscle in different thyroid states. *Jpn J Physiol*. 2001;51:319–326.
4. Konhilas JP, Irving TC, de Tombe PP. Myofilament calcium sensitivity in skinned rat cardiac trabeculae: role of interfilament spacing. *Circ Res*. 2002;90:59–65.
5. Irving TC, Konhilas J, Perry D, et al. Myofilament lattice spacing as a function of sarcomere length in isolated rat myocardium. *Am J Physiol*. 2000;279:H2568–H2573.
6. Yagi N, Shimizu J, Mohri S, et al. X-ray diffraction from a left ventricular wall of rat heart. *Biophys J*. 2004;86:2286–2294.
7. Huxley HE, Brown W. The low-angle x-ray diagram of vertebrate striated muscle and its behaviour during contraction and rigor. *J Mol Biol*. 1967;30:383–434.
8. Sowerby AJ, Harries J, Diakun GP, et al. X-ray diffraction studies of whole rat heart during anoxic perfusion. *Biochem Biophys Res Commun*. 1994;202:1244–1251.
9. Konhilas JP, Irving TC, de Tombe PP. Frank-Starling law of the heart and the cellular mechanisms of length-dependent activation. *Pflugers Arch*. 2002;445:305–310.
10. Ito H, Takaki M, Yamaguchi H, et al. Left ventricular volumetric conductance catheter for rats. *Am J Physiol*. 1996;270:H1509–H1514.
11. Streeter DD Jr, Spotnitz HM, Patel DP, et al. Fiber orientation in the canine left ventricle during diastole and systole. *Circ Res*. 1969;24:339–347.
12. Cecchi G, Bagni MA, Griffiths PJ, et al. Detection of radial cross-bridge force by lattice spacing changes in intact single muscle fibers. *Science*. 1990;250:1409–1411.
13. Bagni M, Cecchi G, Griffiths P, et al. Lattice spacing changes accompanying isometric tension development in intact single muscle fibers. *Biophys J*. 1994;67:1965–1975.
14. Lew WYW, Chen Z, Guth B, et al. Mechanisms of augmented segment shortening in nonischemic areas during acute ischemia of the canine left ventricle. *Circ Res*. 1985;56:351–358.

研　究　論　文

Monochromatic polycapillary imaging utilizing a computed radiography system

Michiaki Sagae[1)*], Eiichi Sato[1)], Yasuomi Hayasi[1)], Etsuro Tanaka[2)], Hidezo Mori[3)], Toshiaki Kawai[4)], Haruo Obara[5)], Toshio Ichimaru[6)], Kazuyoshi Takayama[7)], Hideaki Ido[8)]

[1)] *Department of Physics, Iwate Medical University*
[2)] *Department of Nutritional Science, Faculty of Applied Bio-science, Tokyo University of Agriculture*
[3)] *Department of Cardiac Physiology, National Cardiovascular Center Research Institute*
[4)] *Electron Tube Division #2, Hamamatsu Photonics Inc.*
[5)] *Department of Radiological Technology, College of Medical Science, Tohoku University*
[6)] *Department of Radiological Technology, School of Health Sciences, Hirosaki University*
[7)] *Shock Wave Research Center, Institute of Fluid Science, Tohoku University*
[8)] *Department of Applied Physics and Informatics, Faculty of Engineering, Tohoku Gakuin University*

Research Code No.: 200, 204.1
Key Words: monochromatic radiography, quasi-parallel radiography, x-ray lens, polycapillary plate

Abstract

A fundamental study on quasi-parallel radiography using a polycapillary plate and a copper-target x-ray tube is described. In the experiments, the tube voltage was regulated from 12 to 22 kV, and the tube current was regulated within 3.0 mA by the filament temperature. The exposure time was controlled in order to obtain optimum x-ray intensity, and the maximum focal spot dimensions were approximately 2.0 × 1.5 mm. The thickness and the inner capillary tube diameter of the polycapillary were 1.0 mm and 25 μm, respectively. Monochromatic x-rays were produced using a 10 μm-thick nickel filter with a tube voltage of 17 kV, and these rays were formed into quasi-parallel beams by the polycapillary. The radiogram was taken using a computed

* 岩手医科大学教養部物理学科〔〒020-0015 岩手県盛岡市本町通3-16-1〕: Department of Physics, Iwate Medical University
e-mail: msagae@iwate-med.ac.jp

radiography system utilizing imaging plates. In the measurement of image resolution, the spatial resolution hardly varied according to increases in the distance between the resolution-test chart and imaging plate using a polycapillary. A 50 μm tungsten wire could be observed, and fine blood vessels of approximately 100 μm were visible in angiography.

Received Jan. 7, 2004; revision accepted Jul. 5, 2004

1. Introduction

Monochromatic parallel radiography typically utilizes a synchrotron in conjunction with silicon single crystals and it has been applied in x-ray phase imaging [1-3]. It has also been applied in high contrast micro-angiography [4-7] because x-rays with energies of approximately 35 keV are absorbed effectively by the iodine-based contrast medium.

In order to produce monochromatic x-rays without using the synchrotron, we developed a molybdenum x-ray tube [8] with a transmission-type molybdenum target, which is used as a monochromatic filter for absorbing bremsstrahlung x-rays. In addition, from weakly ionized linear plasma, we found irradiations of intense and sharp characteristic x-rays [9-12].

Recently, several different x-ray lenses [13,14] have been developed, and a polycapillary plate [8-15] has been shown to be useful to perform quasi-parallel radiography with lower photon energy. For this, the plate thickness is about 1 mm, and it is very difficult to design a thicker plate due to technical limitation for increasing the strait capillary length.

In biomedical radiography, because the image processing can be done easily with a Computed Radiography (CR) system [16,17] utilizing imaging plates, the CR system is useful for monochromatic parallel radiography, regardless of whether the image resolution falls as compared with an x-ray film; the spatial resolution is primarily determined by the minimum sampling pitch of 87.5 μm.

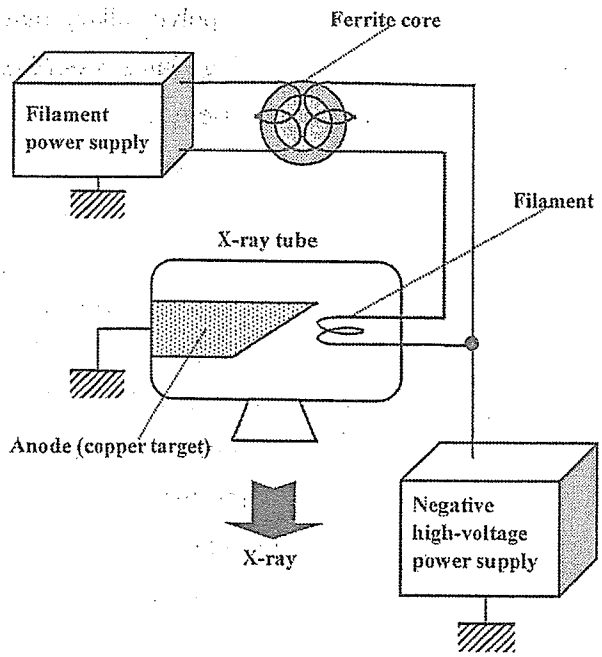

Fig. 1. Circuit diagram of the x-ray generator.

In this article, we describe a monochromatic quasi-parallel radiography system utilizing a polycapillary plate with an inner capilliary diameter of 25 μm, a CR system, and a copper-target radiation tube to realize a low-priced x-ray system utilizing an x-ray lens.

2. Experimental setup

Figure 1 shows the circuit diagram of the x-ray generator, which consists of a negative high-voltage power supply, a filament (hot cathode) power supply, and a copper-target x-ray tube. The negative high voltage is applied to the cathode electrode, and the anode (target) is connected to the ground. In the experiments, the

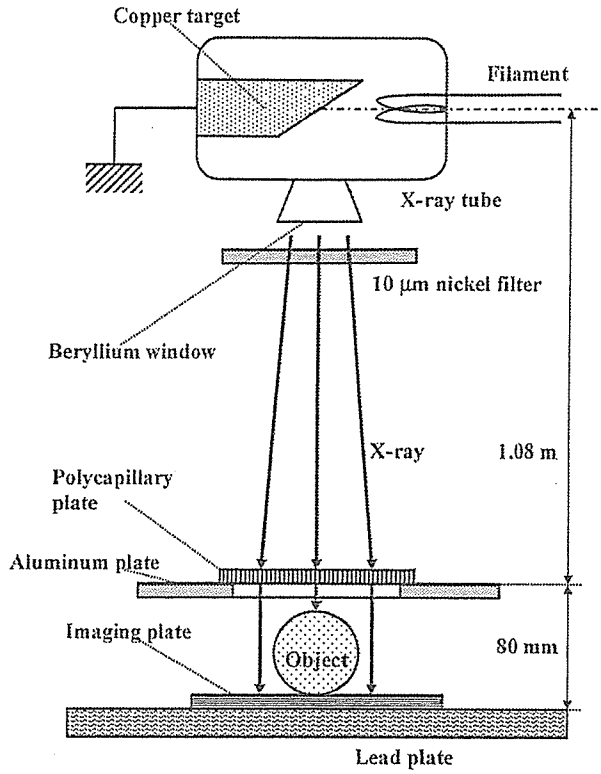

Fig. 2. Experimental setup for polycapillary imaging utilizing a CR system.

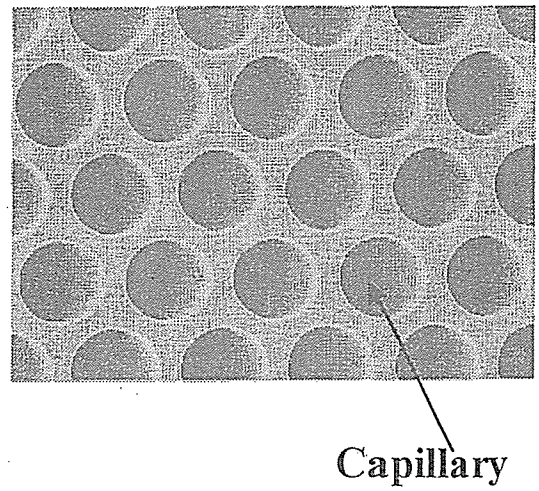

Fig. 3. Polycapillary plate.

tube voltage was regulated from 12 to 22 kV, and the tube current was regulated by the filament temperature and ranged from 1.0 to 3.0 mA. The exposure time was controlled in order to obtain optimum x-ray intensity.

The experimental setup for performing polycapillary imaging is shown in Fig. 2. Monochromatic x-rays were produced using a 10 μm-thick nickel filter, and these rays were formed into quasi-parallel beams by a polycapillary plate (Fig. 3). The polycapillary plate was J5022-21 (Hamamatsu Photonics Inc.), and the plate thickness was 1.0 mm. The outer, effective, and inner capilliary diameters were 87 mm, 77 mm, and 25 μm, respectively. Radiography was performed by a CR system (Konica Regius 150) utilizing imaging plates. The distance between the x-ray source and the polycapillary was 1.08 m, and the polycapillary plate was set on an aluminum plate. The distance between the polycapillary and imaging plates was regulated by the height (30 mm) of the polymethyl methacrylate (PMMA) spacers used.

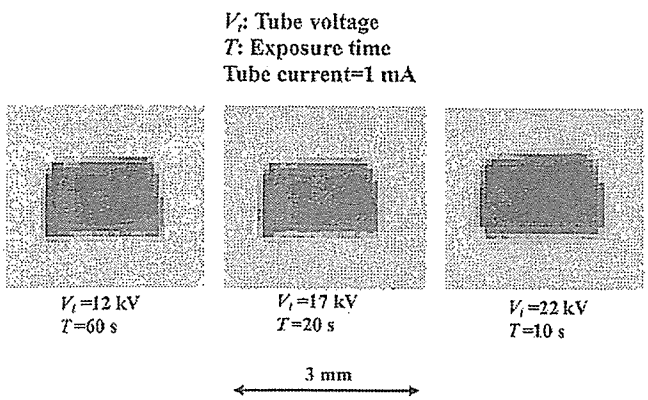

Fig. 4. Images of the x-ray source measured using a 50 μm-diameter pinhole while changing the tube voltage.

3. Characteristics

3.1. Focal spot

In order to measure images of the x-ray source, we employed the CR system, a pinhole camera with a hole diameter of 50 μm, and a filter (Fig. 4). When the tube voltage was increased, the focal spot intensity increased; spot dimensions also increased slightly and were approximately 2.0 × 1.5 mm.

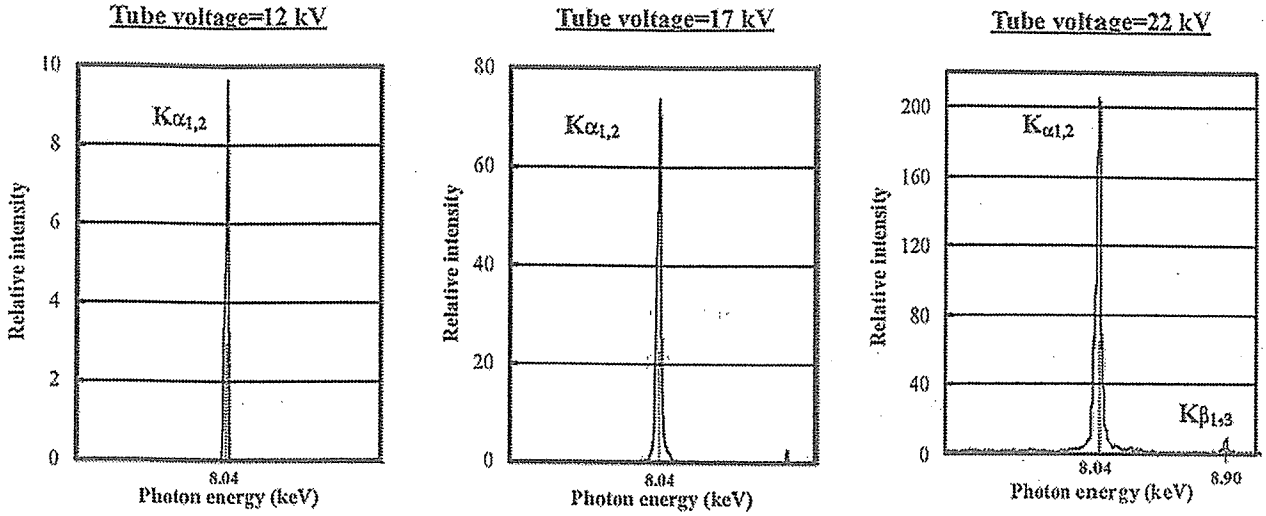

Fig. 5. Measured x-ray spectra while changing the tube voltage.

3.2. *X-ray spectra*

Monochromatic x-ray spectra from the copper-target tube were measured by a transmission-type spectrometer with a lithium fluoride curved crystal 0.5 mm in thickness. The spectra were taken by the CR system with a wide dynamic range, and relative x-ray intensity was calculated from Dicom digital data. Fig. 5 shows measured spectra from the copper target. When the tube voltage was increased, the characteristic x-ray intensity of Kα lines increased.

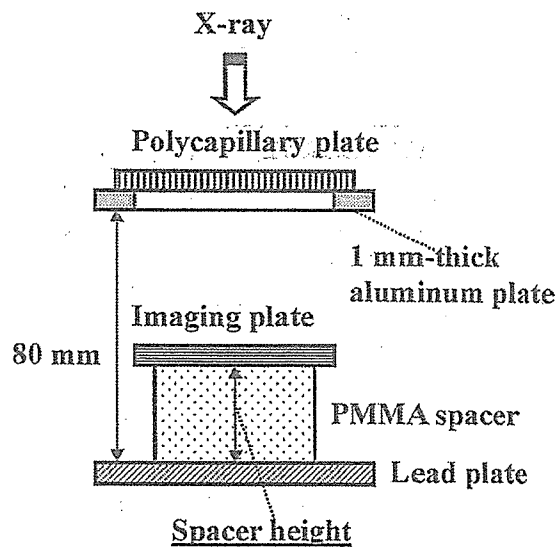

Fig. 6. Radiography for imaging a polycapillary plate while changing the distance between the polycapillary and imaging plates using PMMA spacers.

4. Radiography

The monochromatic radiography was performed with a tube voltage of 17 kV using the filter. Figure 6 shows radiography for imaging a polycapillary plate, and radiograms of the polycapillary are shown in Fig. 7. The center of the black spot in the polycapillary radiogram was mainly imaged by direct transmission beams through capillary holes. As shown in this figure, the spot dimensions increased slightly according to decreases in the PMMA spacer height.

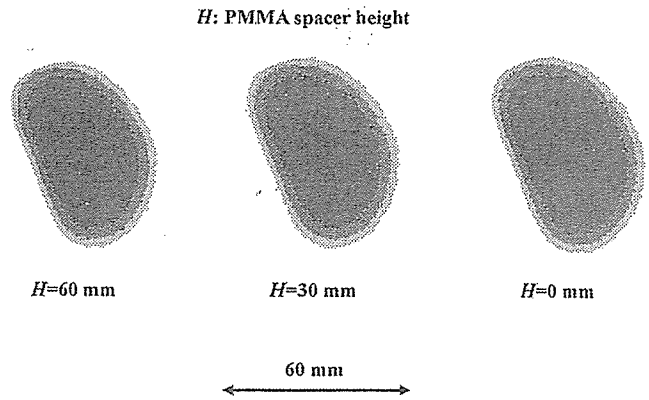

Fig. 7. Radiograms of a polycapillary plate while changing the PMMA height.

Radiography for imaging a test chart for determining image resolution, and the radio-

grams of 166 μm width lead lines, are shown in Figs. 8 and 9, respectively. Both the image resolution and the line contrast fell with decreases in the spacer height. Figure 10 shows the polycapillary radiography for imaging the test chart; the polycapillary was set on the aluminum plate. With this radiography system, we obtained higher contrast lines as compared with those in Fig. 9. When the spacer height was increased, the image resolution hardly varied, and the image dimensions decreased slightly (Fig. 11).

Figures 12 and 13 show radiography and the radiogram of tungsten wires on a PMMA box, respectively. Although the image contrast increased with increases in the wire diameter, a 50 μm-diameter wire could be observed. The angiography for a rabbit heart is shown in Fig 14; iodine-based microspheres of 15 μm diameter were used, and fine blood vessels of about 100 μm were visible (Fig. 15).

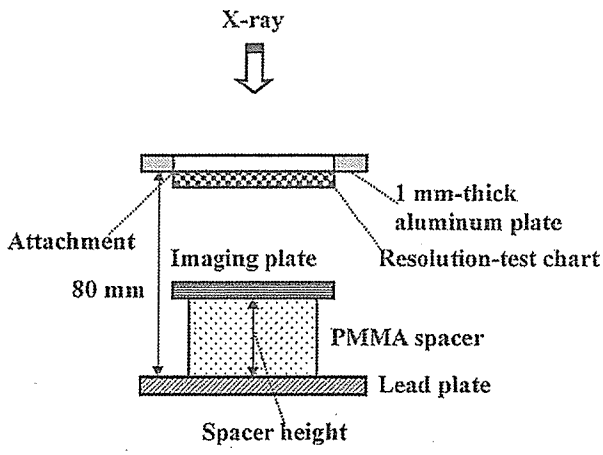

Fig. 8. Radiography for imaging a test chart according to the PMMA spacer height.

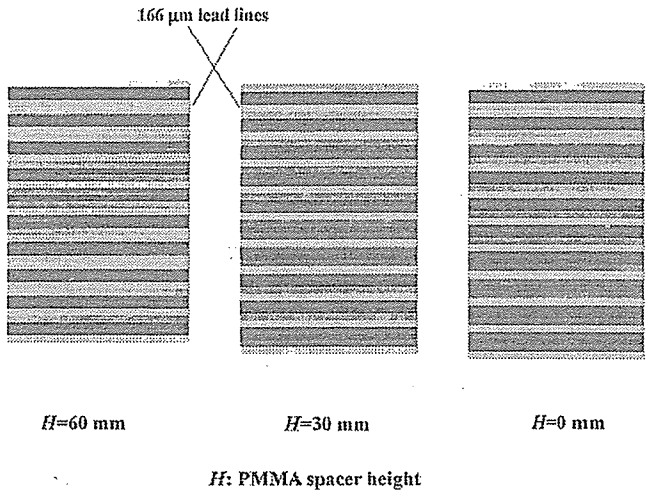

Fig. 9. Radiograms of a test chart according to the PMMA height.

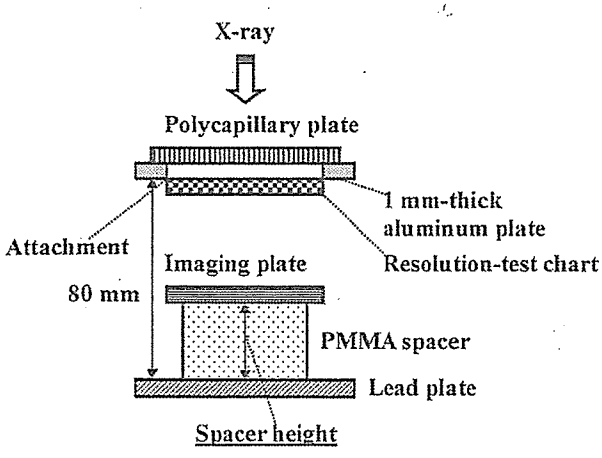

Fig. 10. Radiography for imaging a test chart using a polycapillary plate according to the PMMA height.

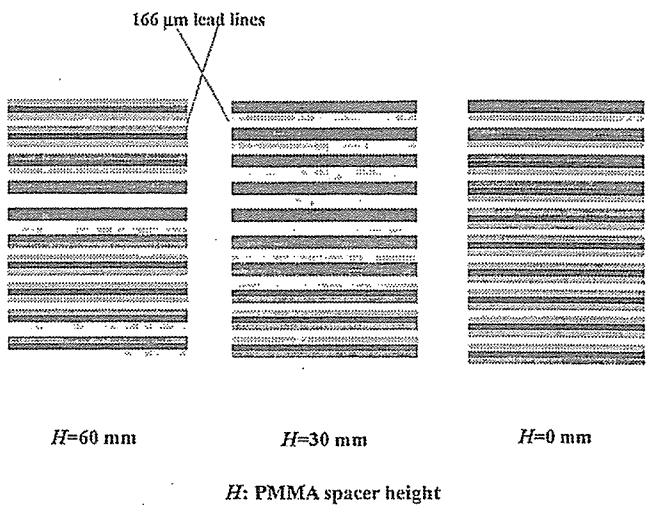

Fig. 11. Radiograms of a test chart using the polycapillary plate according to the PMMA height

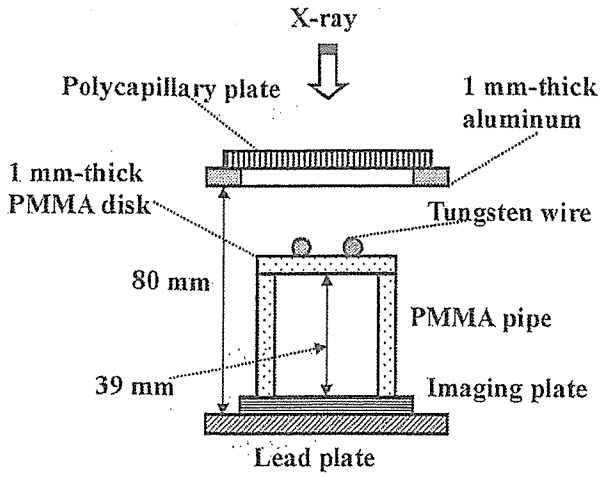

Fig. 12. Radiography for imaging tungsten wires using the polycapillary.

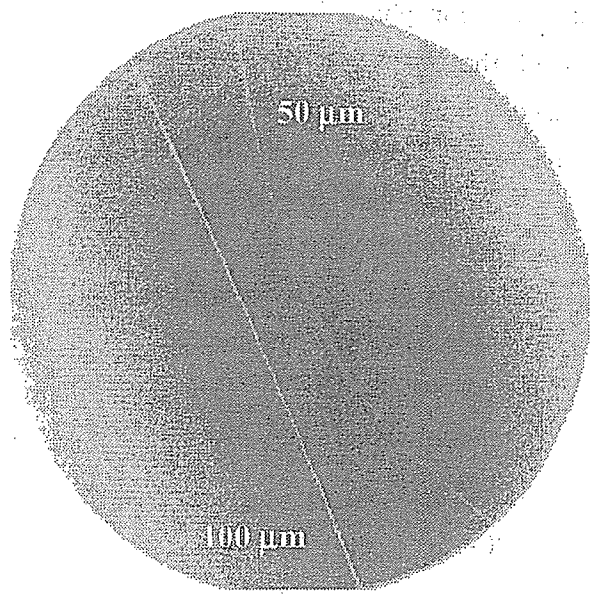

Fig. 13. Radiograms of tungsten wires on a PMMA spacer.

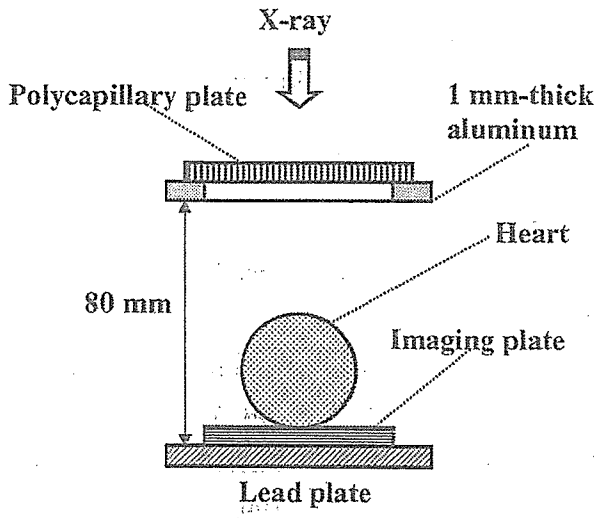

Fig. 14. Angiography using iodine-based microspheres of the heart extracted from a rabbit.

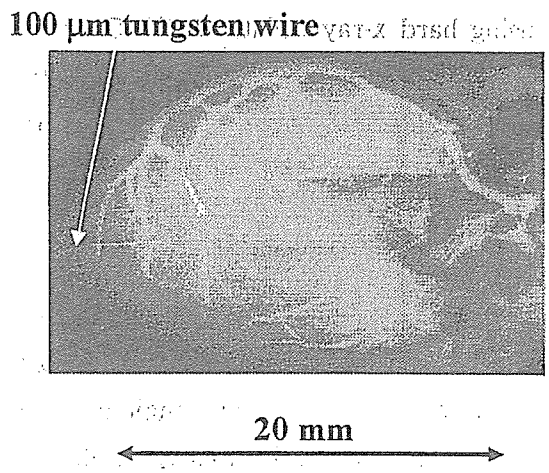

Fig. 15. Angiogram of the heart using the polycapillary.

5. Discussion

In this research, we carried out parallel radiography using a polycapillary plate in conjunction with monochromatic x-rays, and we obtained higher image resolutions as compared with those obtained without using the plate. Currently, the image resolution of the polycapillary is primarily determined by the inner capilliary diameter and the thickness, and it is improved with decreases in the diameter and increases in the thickness. In cases where the CR system is employed, although the resolution of the CR system is primarily determined by the minimum sampling pitch of 87.5 μm, we could observe 50 μm tungsten wires.

The photon energies of the characteristic x-rays are determined by the target element, and the capillary thickness should be increased according to increases in the photon energy because the transmission intensity through capillary glass increases. Subsequently, in order to increase the

parallelity for phase imaging, single crystals should be employed after passing the x-ray beam through the polycapillary.

Since it is possible to increase the irradiation field by increasing the distance between the x-ray source and the polycapillary, this system can be applied to image a wide variety of objects in various fields, including medical radiography.

Acknowledgments

This work was supported by Grants-in-Aid for Scientific Research (13470154, 13877114, and 16591222) and Advanced Medical Scientific Research from MECSST, Grants from Keiryo Research Foundation, The Promotion and Mutual Aid Corporation for Private Schools of Japan, JST (Test of Fostering Potential), NEDO, and MHLW (HLSRG, RAMT-nano-001, RHGTEFB-genome-005, and RGCD13C-1).

References

1) Davis T J, Gao D, Gureyev T E, et al.: Phase-contrast imaging of weakly absorbing materials using hard x-rays. Nature 373: 595-597, 1995
2) Momose A, Takeda T, Itai Y, et al.: Phase-contrast x-ray computed tomography for observing biological soft tissues. Nature Medicine 2: 473-475, 1996
3) Ishisaka A, Ohara H and Honda C: A new method of analyzing edge effect in phase contrast imaging with incoherent x-rays. Opt. Rev. 7: 566-572, 2000
4) Akisada A, Ando M, Hyodo K, Hasegawa S, et al.: An attempt at coronary angiography with a large size monochromatic SR beam. Nucl. Instrum. Meth. Phys. Res. A246: 713-718, 1986
5) Thompson A C, Zeman H D, Brown G S, et al.: First operation of the medical research facility at the NSLS for coronary angiography. Rev. Sci. Instrum. 63: 625-628, 1992
6) Mori H, Hyodo K, Tanaka E, et al.: Small-vessel radiography in situ with monochromatic synchrotron radiation. Radiology 201: 173-177, 1996
7) Hyodo K, Ando M, Oku Y, et al.: Development of a two-dimensional imaging system for clinical applications of intravenous coronary angiography using intense synchrotron radiation produced by a multipole wiggler. J. Synchrotron Rad. 5: 1123-1126, 1998
8) Sato E, Komatsu M, Hayasi Y, et al.: Quasi-monochromatic parallel radiography achieved with a plane-focus x-ray tube. SPIE 4786: 151-161, 2002
9) Sato E, Sagae M, Ichimaru T, et al.: Tentative study on x-ray enhancement by fluorescent emission of radiation by plasma x-ray source. SPIE 3771: 51-60, 1999
10) Sato E, Hayasi Y, Germer R, et al.: Intense characteristic x-ray irradiation from weakly ionized linear plasma and applications. Jpn. J. Med. Imag. Inform. Sci. 20: 148-155, 2003
11) Sato E, Hayasi Y, Germer R, et al.: Irradiation of intense characteristic x-rays from weakly ionized linear molybdenum plasma. Jpn. J. Med. Phys. 23: 123-131, 2003
12) Sato E, Hayasi Y, Germer R, et al.: Quasi-monochromatic flash x-ray generator utilizing weakly

ionized linear copper plasma. Rev. Sci. Instrum. 74: 5236-5240, 2003

13) Xiao Q F and Poturaef S V: Polycapillary-based x-ray optics. Nucl. Instr. Meth. Phys. Res. A 347: 376-383, 1994

14) MacDonald C A, Mail N, Li D, et al.: Monochromatic applications of polycapillary optics. SPIE 5196: 405-411, 2002

15) Sato E, Germer R, Hayasi Y, et al.: Quasi-monochromatic parallel flash radiography achieved with a plane-focus x-ray tube. SPIE 4948: 646-651, 2002

16) Sonoda M, Takano M, Miyahara J, et al.: Computed radiography utilizing scanning laser stimulated luminescence. Radiology 148: 833-838, 1983

17) Sato E, Sato K and Tamakawa Y: Film-less computed radiography system for high-speed imaging. Ann. Rep. Iwate Med. Univ. Sch. Lib. Arts and Sci. 35: 13-23, 2000

Optimal Windows of Statin Use for Immediate Infarct Limitation

5′-Nucleotidase as Another Downstream Molecule of Phosphatidylinositol 3-Kinase

Shoji Sanada, MD, PhD; Hiroshi Asanuma, MD, PhD; Tetsuo Minamino, MD, PhD; Koichi Node, MD, PhD; Seiji Takashima, MD, PhD; Hiroko Okuda, PhD; Yoshiro Shinozaki, MD, PhD; Akiko Ogai, PhD; Masashi Fujita, MD; Akio Hirata, MD; Jiyoong Kim, MD; Yoshihiro Asano, MD, PhD; Hidezo Mori, MD, PhD; Hitonobu Tomoike, MD, PhD; Soichiro Kitamura, MD, PhD; Masatsugu Hori, MD, PhD; Masafumi Kitakaze, MD, PhD

Background—Although statins are reported to have a cardioprotective effect, their immediate direct influence on ischemia-reperfusion injury and the underlying mechanisms remain obscure. We investigated these issues an in vivo canine model.

Methods and Results—Dogs were subjected to coronary occlusion (90 minutes) and reperfusion (6 hours) immediately after injection of pravastatin (0.2, 2, or 10 mg/kg), pitavastatin (0.01, 0.1, or 0.5 mg/kg), or cerivastatin (0.5, 5, or 50 μg/kg). Then myocardial phosphatidylinositol 3-kinase (PI3-K) and 5′-nucleotidase activities were measured, as well as infarct size. After 15 minutes of reperfusion, pravastatin caused dose-dependent activation of Akt and ecto-5′-nucleotidase in the ischemic zone, and the effect was significant at higher doses. Pitavastatin also significantly increased these activities, and its optimal dose was within the clinical range, whereas cerivastatin caused activation at the lowest dose tested. In all cases, both Akt and ecto-5′-nucleotidase showed activation in parallel, and this activation was completely abolished by wortmannin, a PI3-K inhibitor. The magnitude of the infarct-limiting effect paralleled the increase in Akt and ecto-5′-nucleotidase activity and was blunted by administration of wortmannin, α,β-methyleneadenosine-5′-diphosphate, or 8-sulfophenyltheophylline during reperfusion. Both collateral flow and the area at risk were comparable for all groups.

Conclusions—Activation of ecto-5′-nucleotidase after ischemia by PI3-K activation may be crucial for immediate infarct-size limitation by statins. There seems to be an optimal dose for each statin that is independent of its clinical cholesterol-lowering effect. (***Circulation.*** **2004;110:2143-2149.)**

Key Words: statins ■ myocardial infarction ■ adenosine ■ enzymes ■ phosphates

The 3-hydroxy-3-methylglutaryl coenzyme A reductase inhibitors (statins) block the biosynthesis of cholesterol[1] and are widely used clinically to decrease serum cholesterol levels. Recent studies have focused on the pleiotropic effects of either hydrophilic[2-4] or hydrophobic[4,5] statins, which are independent of their cholesterol-lowering effect.[2-4,5] Protection against ischemia-reperfusion injury is one of them, which is particularly evident after 12 hours.[6,7] In addition, some studies showed that statins activate the phosphatidylinositol 3-kinase (PI3-K)/Akt pathway within 1 hour,[8,9] as well as activating endothelial nitric oxide synthase (eNOS),[9,10] to cause immediate infarct limitation.[9]

On the other hand, other studies revealed that statins also acutely activate ecto-5′-nucleotidase,[11] which produces the endogenous cardioprotective substance adenosine,[12] especially in response to certain stresses.[13] Ecto-5′-nucleotidase can act only when localized on the cell membrane,[13] and the density of this enzyme on the membrane regulates its activity.[11,14] Endocytotic turnover of ecto-5′-nucleotidase (5′-nucleotidase localized on the cell surface) is inhibited by PI3-K activation,[14] which subsequently increases total 5′-nucleotidase activity within a period as short as 10 minutes.[14] Therefore, we hypothesized that an increase of ecto-5′-nucleotidase activity might be critical for early cardioprotec-

Received March 26, 2004; revision received May 4, 2004; accepted May 7, 2004

From the Department of Internal Medicine and Therapeutics (S.S., H.A., T.M., S.T., H.O., M.F., A.H., Y.A., M.H.), Osaka University Graduate School of Medicine, Suita; the Department of Cardiovascular and Renal Medicine (K.N.), Saga University Faculty of Medicine, Saga; the Department of Physiological Science (Y.S.), Tokai University School of Medicine, Isehara; and the Cardiovascular Division of Medicine (A.O., J.K., H.M., H.T., S.K., M.K.), National Cardiovascular Center, Suita, Japan

Correspondence to Masafumi Kitakaze, MD, PhD, Director, Cardiovascular Division of Medicine, National Cardiovascular Center, 5-7-1 Fujishirodai, Suita, 565-8565 Japan. E-mail kitakaze@zf6.so-net.ne.jp

Circulation is available at http://www.circulationaha.org

DOI: 10.1161/01.CIR.0000143830.59419.73

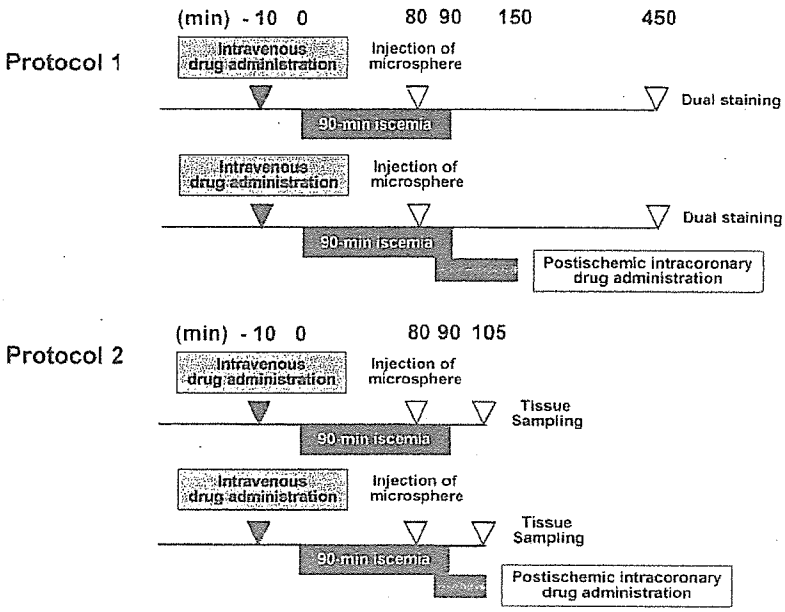

Figure 1. Experimental protocols to measure infarct size (protocol 1; Upper) and kinase activity (protocol 2; Lower).

tion mediated by statins and might be associated with rapid activation of PI3-K.

Here we used a dog model to determine whether 3 statins with different water solubilities (pravastatin, pitavastatin, and cerivastatin) could acutely limit infarct size, as well as whether adenosine and PI3-K were involved in the underlying mechanism.

Methods

All procedures were performed in conformity with the *Guide for the Care and Use of Laboratory Animals* (NIH publication No. 85-23, 1996 revision) and were approved by the Osaka University Committee for Laboratory Animal Use. Pravastatin, pitavastatin, and cerivastatin were obtained from Sankyo, Kowa, and Takeda Pharmaceuticals, respectively. The other drugs were obtained from Sigma.

Instrumentation

Beagle dogs weighing 8 to 13 kg were anesthetized and connected to an extracorporeal bypass tube as described previously.[15,16] In all experiments, the average baseline values of mean aortic blood pressure (ABP), heart rate (HR), and arterial blood Po_2 were 102±2.2 mm Hg, 129±2.5 min^{-1}, and 109±4.1 mm Hg, respectively. Both ABP and HR were measured continuously during the study.

Experimental Protocols

Protocol 1: Measurement of Infarct Size and Myocardial Collateral Blood Flow

After hemodynamic stabilization, we infused pravastatin (0.2, 2, or 10 mg/kg), pitavastatin (0.01, 0.1, or 0.5 mg/kg), cerivastatin (0.5, 5, or 50 μg/kg) or saline intravenously for 10 minutes before 90 minutes of sustained ischemia, which was followed by 6 hours of reperfusion (n=9 to 13 each). Some groups also received intracoronary administration of a selective ecto-5′-nucleotidase inhibitor (α,β-methyleneadenosine-5′-diphosphate [AMP-CP; 80 $\mu g \cdot kg^{-1} \cdot min^{-1}$]; a nonselective adenosine receptor antagonist (8-sulfophenyltheophylline [8-SPT; 50 $\mu g \cdot kg^{-1} \cdot min^{-1}$]); or a selective PI3-K inhibitor (wortmannin [1.5 $\mu g \cdot kg^{-1} \cdot min^{-1}$]) between 5 minutes before and 60 minutes after reperfusion. We measured infarct size and regional myocardial collateral blood flow during 90 minutes of ischemia as described previously.[15]

We have already confirmed in the same model that the doses of AMP-CP,[17] 8-SPT,[17,18] or wortmannin[19] used in this study were appropriate to block ecto-5′-nucleotidase, the adenosine receptors, or PI3-K, respectively. Figure 1 shows the details of this protocol, and the Table lists all of the groups studied.

Protocol 2: Myocardial Enzyme Assays

Another 54 dogs underwent a procedure identical to that of some groups from protocol 1 and were studied for enzyme assays (n=3 or 4 each). In this protocol, not only wortmannin (1.5 $\mu g \cdot kg^{-1} \cdot min^{-1}$) but also LY294002 (60 $\mu g \cdot kg^{-1} \cdot min^{-1}$) was used as another selective PI3-K inhibitor. After 15 minutes of reperfusion, a myocardial tissue sample was obtained from the ischemic border zone to ensure evaluation of viable ischemic myocardium and was used for the measurement of PI3-K and ecto-/endo-5′-nucleotidase activity. The myocardial tissue was rapidly frozen in LN_2 and stored at −80°C. Measurement of PI3-K and 5′-nucleotidase activity was done as reported previously[15,19] with minor modifications.

Criteria for Exclusion

To ensure that all of the animals included in analysis were healthy and were exposed to a similar extent of ischemia, the exclusion criteria reported previously[16] for hemodynamics, excessive collateral flow, and lethal arrhythmia were adopted.

Statistical Analysis

Results were expressed as mean±SEM, and the number of animals or experiments is shown as n. Statistical analysis was performed by ANOVA with a modified Bonferroni post hoc test, and significance was defined at $P<0.05$.

Results

Mortality and Exclusions in Protocol 1

Among 222 dogs used in protocols 1, 56 dogs met the exclusion criteria of ventricular fibrillation or excessive myocardial collateral blood flow (>15 mL · 100 $g^{-1} \cdot min^{-1}$). Therefore, 166 dogs completed these protocols satisfactorily and were included in the data analysis (Table).

Changes in Hemodynamic Parameters, Risk Area, and Collateral Blood Flow in Protocol 1

The changes in ABP and HR were comparable among all groups throughout the protocol (data not shown), and both the

TABLE 1. Mortality, Exclusion, Area at Risk, and Collateral Flow in Each Group in Protocol 1

Groups	Initial No.	Excluded: Lethal Arrhythmia: During Ischemia	Excluded: Lethal Arrhythmia: After Reperfusion	Excluded: Excessive Collateral Flow	Final No.	Area at Risk, %	Collateral Flow, mL/100 g per minute
Control	13	1	2	1	9	40.1±2.1	8.2±1.0
Prava							
0.2	9	0	1	0	8	38.8±2.0	8.4±1.2
2.0	10	0	0	2	8	39.1±2.2	8.9±1.1
10	10	0	0	2	8	39.6±2.1	8.9±1.4
Pitava							
0.01	9	1	1	0	7	38.7±2.2	8.1±1.3
0.1	11	0	1	2	8	39.3±2.0	9.2±1.5
0.5	10	1	0	2	7	39.9±1.9	8.8±1.5
Ceriva							
0.5	11	0	1	2	8	39.2±1.9	8.5±1.3
5.0	10	1	1	1	7	38.9±2.1	8.7±1.4
50	11	0	1	3	7	39.0±2.0	9.1±1.5
AMP-CP							
+Prava 10	9	0	2	0	7	40.4±2.3	8.6±1.3
+Pitava 0.1	9	0	1	1	7	39.8±2.0	8.4±1.5
+Ceriva 0.5	9	1	1	0	7	40.4±2.3	9.0±1.4
8SPT							
+Prava 10	10	0	1	1	8	38.7±2.2	8.3±1.3
+Pitava 0.1	11	1	2	0	8	39.9±2.1	8.2±1.6
+Ceriva 0.5	11	0	2	1	8	38.4±2.6	8.5±1.5
WTMN							
+Prava 10	10	0	2	1	7	38.6±2.3	9.5±1.5
+Pitava 0.1	10	0	2	0	8	38.9±2.1	9.2±1.6
+Ceriva 0.5	10	0	1	1	8	39.8±2.8	8.8±1.4
AMP-CP	9	0	2	0	7	38.8±2.5	8.5±1.6
8SPT	11	0	3	0	8	39.6±2.5	8.2±1.5
WTMN	9	1	2	0	6	40.5±2.3	8.6±1.6

Data expressed as mean±SEM. Prava indicates pravastatin (mg/kg); Pitava, pitavastatin (mg/kg); Ceriva, cerivastatin (μg/kg); 8SPT, 8-sulfophenyltheophilline; and WTMN, wortmannin.

area at risk and collateral blood flow were also comparable (Table).

Infarct Size

Figure 2 shows infarct size in the groups of protocol 1. Pravastatin (0.2, 2, and 10 mg/kg) dose-dependently reduced the infarct size (29.5±3.5%, 22.5±4.0%, and 18.8±3.4%, respectively) compared with that in the control group (39.8±3.6%), and the difference was significant at 2 mg/kg or more. Pitavastatin (0.01, 0.1, and 0.5 mg/kg) also reduced infarct size (32.9±3.9%, 23.6±3.8%, and 31.4±3.9%, respectively), although the optimal dose was 0.1 mg/kg (the only dose that produced a significant difference). Although cerivastatin (0.5, 5, and 50 μg/kg) caused infarct limitation (26.2±3.2%, 32.1±5.3%, and 37.1±4.4%, respectively), it was significant at the lowest dose only, and the effect was weaker at higher doses. Furthermore, cotreatment with AMP-CP, 8-SPT, or wortmannin between 5 minutes before and 60 minutes after reperfusion abrogated the infarct-limiting effect of pravastatin (39.9±4.0%, 42.6±4.0%, or 38.6±3.6%, respectively), pitavastatin (40.4±3.1%, 39.4±3.6%, or 39.1±3.1%, respectively), and cerivastatin (41.1±3.7%, 42.1±3.9%, or 40.4±4.0%, respectively), although these drugs per se did not affect infarct size (42.7±4.5%, 40.3±3.5%, or 42.7±4.5%, respectively).

5′-Nucleotidase Activity at Reperfusion

Figure 3 shows the activity of ecto-/endo-5′-nucleotidase in protocol 2. Sustained ischemia for 90 minutes and 15 minutes of subsequent reperfusion did not significantly change the activity of ecto-5′-nucleotidase (41.0±5.7 versus 33.2±1.2 nmol · mg protein^{-1} · min^{-1} at baseline). Preischemic treat-

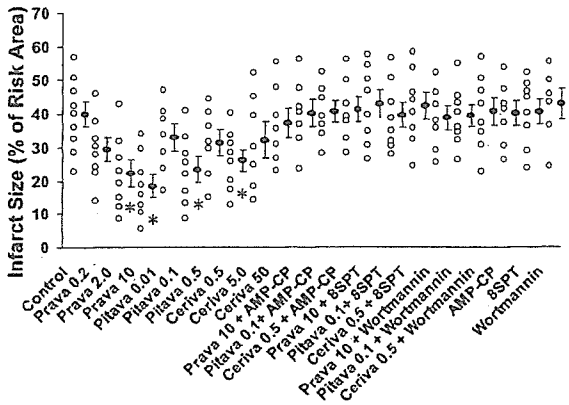

Figure 2. Infarct size in each group in protocol 1. Data are expressed as mean±SEM. *$P<0.05$ vs control. Open circles show infarct size in each individual. Prava indicates pravastatin; Pitava, pitavastatin; and Ceriva; cerivastatin. All other abbreviations are as defined in text.

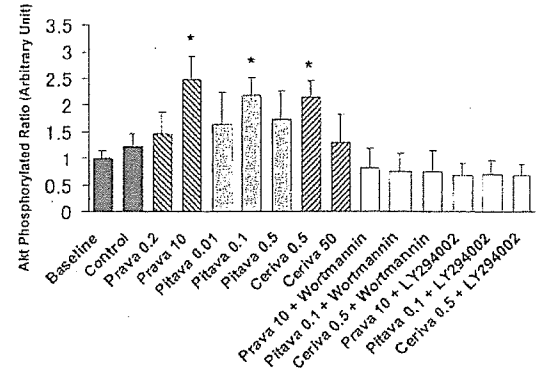

Figure 4. Myocardial PI3-K activity represented by phosphorylated ratio of Akt in each group in protocol 2. Data are expressed as mean±SEM. n=4 each, *$P<0.05$ vs control. Abbreviations are as defined in text and in legend to Figure 2.

ment with pravastatin caused a dose-dependent and acute increase of ecto-5′-nucleotidase activity in the ischemic zone, which became significant at the highest dose (72.6±6.0 nmol · mg protein^{-1} · min^{-1} at 10 mg/kg, $P<0.05$ versus control). Pitavastatin also caused significant activation at its optimal (medium) dose (66.7±6.1 nmol · mg protein^{-1} · min^{-1} at 0.1 mg/kg, $P<0.05$ versus control). Cerivastatin caused activation at the lowest dose (62.5±5.6 nmol · mg protein^{-1} · min^{-1} at 0.5 μg/kg, $P<0.05$ versus control). All of these increases were canceled by the selective PI3-K inhibitors wortmannin (39.5±6.8 nmol · mg protein^{-1} · min^{-1} for pravastatin, 37.0±7.1 nmol · mg protein^{-1} · min^{-1} for pitavastatin, and 38.4±6.5 nmol · mg protein^{-1} · min^{-1} for cerivastatin) or LY294002 (33.5±6.5 nmol · mg protein^{-1} · min^{-1} for pravastatin, 35.0±6.2 nmol · mg protein^{-1} · min^{-1} for pitavastatin, and 37.5±6.7 nmol · mg protein^{-1} · min^{-1} for cerivastatin). The activity of endo-5′-nucleotidase remained unchanged in all cases.

PI3-K Activity at Reperfusion

Figure 4 shows the activity of PI3-K in protocol 2. Sustained ischemia for 90 minutes and subsequent reperfusion for 15 minutes did not change PI3-K activity significantly (123±23% versus 100±14% at baseline). Preischemic treatment with pravastatin caused dose-dependent and acute activation of ecto-5′-nucleotidase in the ischemic zone, which was significant at the highest dose (249±44% at 10 mg/kg, $P<0.05$ versus control). Pitavastatin also caused significant activation at its medium dose (218±34% at 0.1 mg/kg, $P<0.05$ versus control), whereas cerivastatin caused activation at the lowest dose (214±31% at 0.5 μg/kg, $P<0.05$ versus control). We confirmed that all of these increases were also blocked by wortmannin (81±38% for pravastatin,

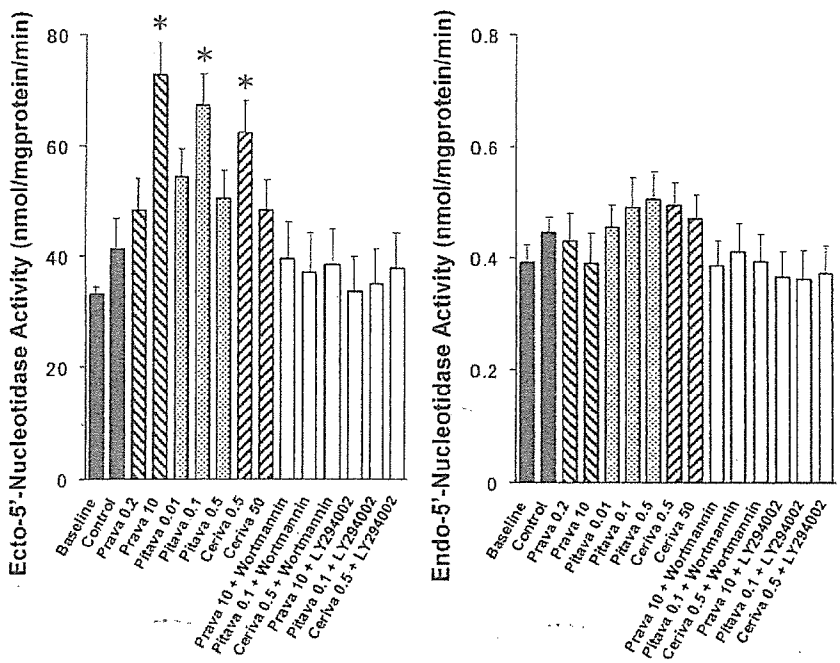

Figure 3. Myocardial ecto-/endo-5′-nucleotidase activity in each group in protocol 2. Data are expressed as mean±SEM. n=4 each, *$P<0.05$ vs control. Abbreviations are as defined in text and in legend to Figure 2.

77±32% for pitavastatin, and 76±39% for cerivastatin) or LY294002 (69±23% for pravastatin, 70±27% for pitavastatin, and 68±21% for cerivastatin).

Discussion

The present study demonstrates that several statins provide immediate infarct limitation of different magnitudes and at different optimal doses. Our results also suggest that activation of ecto-5′-nucleotidase through the activation of PI3-K after ischemia was involved in this cardioprotective mechanism of statins.

Cholesterol-Lowering Effects and Immediate Infarct Limitation of Statins

In this study, we set the doses of statins in line with their clinical cholesterol-lowering properties. In Japan, the standard clinical doses to obtain a 20% to 30% reduction of total plasma cholesterol levels were 10 mg/d for pravastatin, 2 mg/d for pitavastatin, and 0.15 mg/d for cerivastatin. Our preliminary trials in the same dog model revealed that a single intravenous injection of 0.2 mg/kg pravastatin, 0.1 mg/kg pitavastatin, or 5 μg/kg cerivastatin approximated the clinical cholesterol-lowering dose based on the maximal plasma concentration of each statin (data not shown). Because (1) the maximal infarct limitation was achieved by a higher dose of pravastatin than the clinical dose, whereas the dose was similar to the clinical dose for pitavastatin and lower for cerivastatin, and (2) these statins showed early cardioprotection within 2 hours of administration in this model, it is strongly suggested that the magnitude of immediate infarct limitation by each statin is not correlated with its cholesterol-lowering effect.

Existence of Optimal Cardioprotective Doses for Each Statin

In the present report, we have directly shown that pitavastatin has the optimal dose to reduce infarct size. Obviously, there is also an optimal dose for cerivastatin under the lowest dose we tried, because infarct size with far lower doses of cerivastatin near zero will converge with those of control levels. In the case of pravastatin, our additional experiment, within the limitation with regard to the total amount of the drug we could obtain, showed that 100 mg/kg pravastatin administered in the same manner as in protocol 1 exerted similar (but a slightly weaker) magnitude of reducing infarct size (20.9±4.5%, n=5) compared with that achieved with 10 mg/kg of this agent. Although we could not show direct evidence in this case, it would at least not deny the possibility for the existence of an optimal dose of pravastatin. Furthermore, other reports also showed the existence of an optimal dose of atorvastatin for infarct limitation[9] or of simvastatin for PI3-K activation.[8] Taken together, the existence of optimal doses should be ubiquitous among all (or at least all hydrophobic) statins.

Although direct exhibition of the reason for this phenomenon remains unclear in this study, there might be some reasons to regulate the respective optimal windows for each statin, eg, differences in the ability to attenuate inflammatory response[20] or in the potency of direct absorption into cellular membrane to modulate intracellular signaling systems. In addition, our present finding that infarct limitation completely paralleled the activation of PI3-K leads us to hypothesize that the lesser effects by the higher doses of statins should be regulated upstream of PI3-K. One possibility is that all hydrophobic statins can dose-dependently activate apoptosis-related signals,[21] which might also explain the wide range of higher cardioprotective doses for pravastatin specifically. Finally, additional studies will need to be performed to obtain direct evidence.

Cardioprotective Mechanisms

Our observations that (1) activation of PI3-K and ecto-5′-nucleotidase was coincident with a substantial limitation of infarct size, (2) either wortmannin or AMP-CP abolished cardioprotection by all 3 statins, (3) different PI3-K inhibitors at reperfusion actually inhibited PI3-K activity (Figure 4) and subsequently reduced ecto-5′-nucleotidase activity (Figure 3), and (4) our preliminary documentation that PI3-K inhibition by either wortmannin of LY294002 before ischemia did not abolish the infarct limitation by statins in the present study (n=4 or 5, data not shown), together suggest that infarct limitation in this model was linked to the activation of PI3-K during reperfusion, not before ischemia, followed by ecto-5′-nucleotidase activation.

In this study, we did not determine the exact mechanism of how PI3-K activates ecto-5′-nucleotidase. Although we have previously reported that phosphorylation of ecto-5′-nucleotidase might be crucial,[22] other mechanisms may also be involved, such as endocytotic turnover.[17] In addition, although we did not evaluate real-time regional myocardial production of adenosine in each group, treatment with a potent adenosine receptor antagonist (8-SPT) during reperfusion also blunted infarct limitation by statins along with the inhibition of ecto-5′-nucleotidase, further suggesting that cardioprotection against ischemia-reperfusion injury via ecto-5′-nucleotidase activation might be mediated by an increase of adenosine, the main product of ecto-5′-nucleotidase.[11,13,22] However, other implicated mechanism of enhanced activation of the adenosine receptor (eg, increased receptor sensitivity) should be determined by future studies.

Possible Link Between Cardioprotection by Adenosine and NO

Previous studies support our present findings that statins rapidly activate the PI3-K/Akt pathway,[8,9] and we obtained another preliminary finding that the cotreatment with N^{ω}-nitro-L-arginine methyl ester (10 $\mu g \cdot kg^{-1} \cdot min^{-1}$) in the same manner as in protocol 1, which we confirmed did not affect baseline infarct size in the present model,[23] blunted the infarct limitation by pravastatin (36.8±4.1%, n=7), pitavastatin (39.9±3.9%, n=6), and cerivastatin (42.6±4.6%, n=5). Therefore, there is a possibility that ecto-5′-nucleotidase and NO act in series to cause statin-induced cardioprotection.

Although elucidation of a direct effect should be the focus of future studies, there are at least 2 lines of evidence to support the explanation that adenosine and NO synergistically caused infarct limitation in this study. First, NO directly exerts cardioprotection[24]: NO inhibits cell-to-cell adhesion,

such as that between platelets[25] or between neutrophils and endothelial cells,[26,27] by reducing expression of P-selectin,[27] E-selectin, and intercellular adhesion molecule-1,[28] which leads to attenuation of the inflammatory response[22,24,25] or protects against ischemia-reperfusion injury.[25–28] In addition, NO is reported to inhibit caspase-3 activity and to block apoptosis of cardiac myocytes.[29] On the other hand, adenosine also rescues injured myocardium through activating adenosine receptors.[13,30–32] Either administration of adenosine or enhancement of endogenous adenosine release during reperfusion after sustained ischemia limits infarct size.[13,17] We and others have shown that (1) adenosine receptor (A_1 and A_2) activation improves contractile dysfunction after reperfusion,[14] (2) inhibition of norepinephrine release from the presynaptic vesicles and attenuation of calcium influx occur through the A_1 receptor and the coupled inhibitory G protein,[33,34] (3) inhibition of platelet aggregation and leukocyte activation occurs through the A_2 receptor and the coupled stimulatory G protein,[34–36] and (4) activation of extracellular signal–regulated kinase, one of the reperfusion injury survival kinase pathways,[37] takes place during reperfusion through the A_3 receptor.[38] Therefore, either adenosine or NO similarly and potentially protects injured myocardium through multiple pathways.

Second, recent articles have shown that either adenosine[38–40] or NO[41] can reactivate PI3-K downstream. However, increasing the production of both agents is known to negatively regulate further increases of production of these molecules,[42,43] suggesting the requirement of both pathways to confer sufficient cardioprotection in the physiological system. Taking all of these together, it is likely that adenosine and NO synergistically confer the statin-derived immediate cardioprotection shown in this study.

In conclusion, our findings suggest the cellular mechanism by which statins attenuate myocardial injury, which may indicate the possibility of acute protective therapies for ischemia and associated myocardial stresses.

Acknowledgments

This study was supported by grants on the Human Genome, Tissue Engineering and Food Biotechnology (H13-Genome-11) and grants on Comprehensive Research on Aging and Health (H13-21seiki[seikatsu]-23) in Health and Labor Sciences Research from the Ministry of Health, Labor and Welfare; a grant-in-aid for Scientific Research from the Ministry of Education, Culture, Sports, Science and Technology of Japan; and in part by a grant-in-aid for JSPS fellows from the Japan Society for the Promotion of Science and the Japan Heart Foundation.

References

1. Goldstein JL, Brown MS. Regulation of the mevalonate pathway. *Nature*. 1990;343:425–430.
2. Sacks FM, Pfeffer MA, Moye LA, et al. The effect of pravastatin on coronary events after myocardial infarction in patients with average cholesterol levels: Cholesterol and Recurrent Events Trial investigators. *N Engl J Med*. 1996;335:1001–1009.
3. LIPID Study Group. Prevention of cardiovascular events and death with pravastatin in patients with coronary heart disease and a broad range of initial cholesterol levels: the Long-Term Intervention with Pravastatin in Ischaemic Disease (LIPID) Study Group. *N Engl J Med*. 1998;339:1349–1357.
4. 4S Study Group. Randomized trial of cholesterol lowering in 4444 patients with coronary heart disease: the Scandinavian Simvastatin Survival Study (4S). *Lancet* 1994;344:1383–1389.
5. Downs JR, Clearfield M, Weis S, et al. Primary prevention of acute coronary events with lovastatin in men and women with average cholesterol levels: results of AFCAPS/TexCAPS: Air Force/Texas Coronary Atherosclerosis Prevention Study. *JAMA*. 1998;279:1615–1622.
6. Lefer AM, Campbell B, Shin YK, et al. Simvastatin preserves the ischemic-reperfused myocardium in normocholesterolemic rat hearts. *Circulation*. 1999;100:178–184.
7. Ikeda Y, Young LH, Lefer AM. Rosuvastatin, a new HMG-CoA reductase inhibitor, protects ischemic reperfused myocardium in normocholesterolemic rats. *J Cardiovasc Pharmacol*. 2003;41:649–656.
8. Kureishi Y, Luo Z, Shiojima I, et al. The HMG-CoA reductase inhibitor simvastatin activates the protein kinase Akt and promotes angiogenesis in normocholesterolemic animals. *Nat Med*. 2000;6:1004–1010.
9. Bell RM, Yellon DM. Atorvastatin, administered at the onset of reperfusion, and independent of lipid lowering, protects the myocardium by up-regulating a pro-survival pathway. *J Am Coll Cardiol*. 2003;41:508–515.
10. Simoncini T, Genazzani AR, Liao JK. Nongenomic mechanisms of endothelial nitric oxide synthase activation by the selective estrogen receptor modulator raloxifene. *Circulation*. 2002;105:1368–1373.
11. Ledoux S, Laouari D, Essig M, et al. Lovastatin enhances ecto-5′-nucleotidase activity and cell surface expression in endothelial cells: implication of rho-family GTPases. *Circ Res*. 2002;90:420–427.
12. Kitakaze M, Hori M, Morioka T, et al. α^1-Adrenoceptor activation mediates the infarct size-limiting effect of ischemic preconditioning through augmentation of 5′-nucleotidase activity. *J Clin Invest*. 1994;93:2197–2205.
13. Kitakaze M, Minamino T, Node K, et al. Adenosine and cardioprotection in the diseased heart. *Jpn Circ J*. 1999;63:231–243.
14. Tuma PL, Finnegan CM, Yi JH, et al. Evidence for apical endocytosis in polarized hepatic cells: phosphoinositide 3-kinase inhibitors lead to the lysosomal accumulation of resident apical plasma membrane proteins. *J Cell Biol*. 1999;145:1089–1102.
15. Kitakaze M, Node K, Minamino T, et al. Role of activation of protein kinase C in the infarct size-limiting effect of ischemic preconditioning through activation of ecto-5′-nucleotidase. *Circulation*. 1996;93:781–791.
16. Sanada S, Kitakaze M, Papst PJ, et al. Role of phasic dynamism of P38 mitogen-activated protein kinase activation in the ischemic preconditioning on the canine heart. *Circ Res*. 2001;88:175–180.
17. Kitakaze M, Minamino T, Funaya H, et al. Vesnarinone limits infarct size via adenosine-dependent mechanisms in the canine heart. *Circulation*. 1997;95:2108–2114.
18. Node K, Kitakaze M, Minamino T, et al. Activation of ecto-5′-nucleotidase by protein kinase C and its role in ischaemic tolerance in the canine heart. *Br J Pharmacol*. 1997;120:273–281.
19. Ogita H, Node K, Asanuma H, et al. Raloxifene improves coronary perfusion, cardiac contractility and myocardial metabolism in the ischemic heart: role of phosphatidylinositol 3-kinase/Akt pathway. *J Cardiovasc Pharmacol*. 2004;43:821–829.
20. Hilgendorff A, Muth H, Parviz B, et al. Statins differ in their ability to block NF-κB activation in human blood monocytes. *Int J Clin Pharmacol Ther*. 2003;41:397–401.
21. Kaneta S, Satoh K, Kano S, et al. All hydrophobic HMG-CoA reductase inhibitors induce apoptotic death in rat pulmonary vein endothelial cells. *Atherosclerosis*. 2003;170:237–243.
22. Kitakaze M, Minamino T, Node K, et al. Activation of ecto-5′-nucleotidase and cardioprotection of ischemic preconditioning. *Basic Res Cardiol*. 1996;91:23–26.
23. Asanuma H, Kitakaze M, Funaya H, et al. Nifedipine limits infarct size via NO-dependent mechanisms in dogs. *Basic Res Cardiol*. 2001;96:497–505.
24. Lefer AM, Lefer DJ. Nitric oxide, II: nitric oxide protects in intestinal inflammation. *Am J Physiol*. 1999;276:G572–G575.
25. Massberg S, Sausbier M, Klatt P, et al. Increased adhesion and aggregation of platelets lacking cyclic guanosine 3′,5′-monophosphate kinase I. *J Exp Med*. 1999;189:1255–1264.
26. Agullo L, Garcia-Dorado D, Inserte J, et al. L-Arginine limits myocardial cell death secondary to hypoxia-reoxygenation by a cGMP-dependent mechanism. *Am J Physiol*. 1999;276:H1574–H1580.

27. Jordan JE, Zhao ZQ, Vinten-Johansen J. The role of neutrophils in myocardial ischemia-reperfusion injury. *Cardiovasc Res*. 1999;43: 860–878.
28. Buras JA, Stahl GL, Svoboda KK, et al. Hyperbaric oxygen down-regulates ICAM-1 expression induced by hypoxia and hypoglycemia: the role of NOS. *Am J Physiol Cell Physiol*. 2000;278:C292–C302.
29. Weiland U, Haendeler J, Ihling C, et al. Inhibition of endogenous nitric oxide synthase potentiates ischemia-reperfusion–induced myocardial apoptosis via a caspase-3 dependent pathway. *Cardiovasc Res*. 2000;45: 671–678.
30. Dorheim TA, Hoffman A, Van Wylen DG, et al. Enhanced interstitial fluid adenosine attenuates myocardial stunning. *Surgery*. 1991;110: 136–145.
31. Babbitt DG, Virmani R, Vildibill HD Jr, et al. Intracoronary adenosine administration during reperfusion following 3 hours of ischemia: effects on infarct size, ventricular function, and regional myocardial blood flow. *Am Heart J*. 1990;120:808–818.
32. Norton ED, Jackson EK, Virmani R, et al. Effect of intravenous adenosine on myocardial reperfusion injury in a model with low myocardial collateral blood flow. *Am Heart J*. 1991;122:1283–1291.
33. Richardt G, Waas W, Kranzhofer R, et al. Adenosine inhibits exocytotic release of endogenous noradrenaline in rat heart: a protective mechanism in early myocardial ischemia. *Circ Res*. 1987;61:117–123.
34. Sato H, Hori M, Kitakaze M, et al. Endogenous adenosine blunts β-adrenoceptor–mediated inotropic response in hypoperfused canine myocardium. *Circulation*. 1992;85:1594–1603.
35. Cronstein BN, Levin RI, Belanoff J, et al. Adenosine: an endogenous inhibitor of neutrophil-mediated injury to endothelial cells. *J Clin Invest*. 1986;78:760–770.
36. Kitakaze M, Hori M, Sato H, et al. Endogenous adenosine inhibits platelet aggregation during myocardial ischemia. *Circ Res*. 1991;69:1402–1408.
37. Hausenloy DJ, Yellon DM. New directions for protecting the heart against ischaemia-reperfusion injury: targeting the reperfusion injury salvage kinase (RISK)-pathway. *Cardiovasc Res*. 2004;61:448–460.
38. Trincavelli ML, Tuscano D, Marroni M, et al. Involvement of mitogen protein kinase cascade in agonist-mediated human A_2 adenosine receptor regulation. *Biochim Biophys Acta*. 2002;1591:55–62.
39. Yang XM, Krieg T, Cui L, et al. NECA and bradykinin at reperfusion reduce infarction in rabbit hearts by signaling through PI3K, ERK, and NO. *J Mol Cell Cardiol*. 2004;36:411–421.
40. Boucher M, Pesant S, Falcao S, et al. Post-ischemic cardioprotection by A2A adenosine receptors: dependent of phosphatidylinositol 3-kinase pathway. *J Cardiovasc Pharmacol*. 2004;43:416–422.
41. Kawasaki K, Smith RS Jr, Hsieh CM, et al. Activation of the phosphatidylinositol 3-kinase/protein kinase Akt pathway mediates nitric oxide–induced endothelial cell migration and angiogenesis. *Mol Cell Biol*. 2003;23:5726–5737.
42. Richardt G, Waas W, Kranzhofer R, et al. Interaction between the release of adenosine and noradrenaline during sympathetic stimulation: a feed-back mechanism in rat heart. *J Mol Cell Cardiol*. 1989;21:269–277.
43. Buga GM, Griscavage JM, Rogers NE, et al. Negative feedback regulation of endothelial cell function by nitric oxide. *Circ Res*. 1993;73: 808–812.